Performance of Angle-of-Arrival Algorithms for an Inflight Triple-GEM Detector

Michael Luntz, Marcus Hohlmann, Devon Madden

High Energy Physics Group

Aerospace, Physics & Space Sciences Dept.

Florida Institute of Technology

RD51 Note 2022-xx

Abstract

In this paper we report on the results of a study of algorithms to determine the angle of arrival (AOA) of charged particles impinging on a Triple-GEM detector with a 16 mm drift gap using data collected at Fermilab by a group of researchers from Brookhaven National Laboratory (BNL). The focus of the study was on algorithms that use detected pulse time of arrival (TOA) versus readout strip to reconstruct a straight track for the particle. Combining the track reconstructions from the x and y projections enables computing the AOA in 3D space. A number of TOA measurement approaches were evaluated for their impact on the AOA angular resolution. Using the TOA algorithm resulting in the best resolution, the AOA resolution ranged between 0.53° and 0.77° when the track was not directly aligned with either the x or y readout strips. These results have been compared, to the degree possible, with results independently reported by BNL. When using a TOA estimate algorithm similar to that which BNL used, our results for individual x-channel and y-channel resolutions roughly matched theirs. An improved TOA measurement algorithm is presented here that was found to provide about 10%-20% better angular resolution than reported by BNL. The BNL data were also used to predict the resolution achievable over a range of drift gap widths. Using a 3 mm drift gap, with an angle of incidence of 45°, the angular resolution is estimated to be on the order of 6° and 12° for the polar and azimuthal angles respectively. Increasing the drift gap to 9 mm the angular resolution was found to decrease to within 1° to 1.5° of the resolution when using a 16 mm drift gap, and with a 12 mm drift gap full resolution is predicted. The TOA based approach is only possible when the angle of the track does not coincide with either the x or y readout strips. Most of these results were computed for relatively large beam track angles with respect to the readout strips. For cases in which the beam track aligns with one or both readout strips, some simple algorithms not requiring measurement of TOA, similar to those used by BNL were also evaluated. Using these algorithms, the AOA resolution was found to be on the order of 1.3°.

Introduction

High energy extraterrestrial particles lose energy in the atmosphere before reaching the ground so they are not normally a health concern. But in the high-altitude flight or space environment these particles have the capability of harming humans or damaging sensitive equipment. Strategically located shielding can protect occupants and equipment from damage, and to determine where to locate this shielding requires knowing the direction of these incoming particles. The envisioned function of the in-flight detector is to measure the direction of arrival of these particles to aid in designing the shielding.

In-flight Detector Description

A gas electron multiplier (GEM) detector [1] can be used to measure the direction of arrival of charged particles. A GEM detector is made up of a stack of electrodes, including a top electrode, also known as the drift electrode, one or more electron multiplier electrodes, also known as GEM foils, and a charge collection electrode as shown in Figure 1. A high voltage applied between the top electrode and the charge collection electrode is distributed through the detector using a resistor network. The entire space between the top and charge collection electrodes is filled with a gas such as a mixture of Argon and CO_2. In the space between the top electrode and the first electron multiplier electrode, called the drift region, incoming charged particles can ionize the gas molecules releasing electrons which drift under an electric field toward the first electron multiplier electrode. The electron multiplier consists of top and bottom electrodes punctured with microscopic holes across which a high electric field is applied. Electrons entering these holes are accelerated and this added energy enables the electron to ionize additional gas molecules, thus multiplying the number of electrons released for each gas molecule ionized by the original particle. At the bottom of the stack are a set of 2-dimensional charge collection readout strips connected to amplifiers whose pulse output voltage is proportional to the charge collected on the readout strips. Readout of

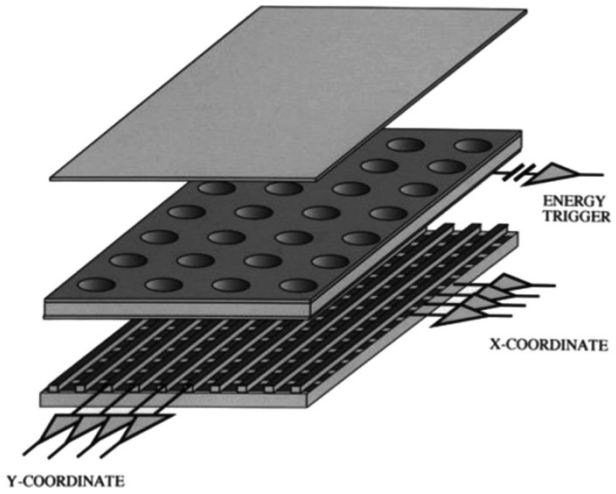

Figure 1. GEM detector components [1]

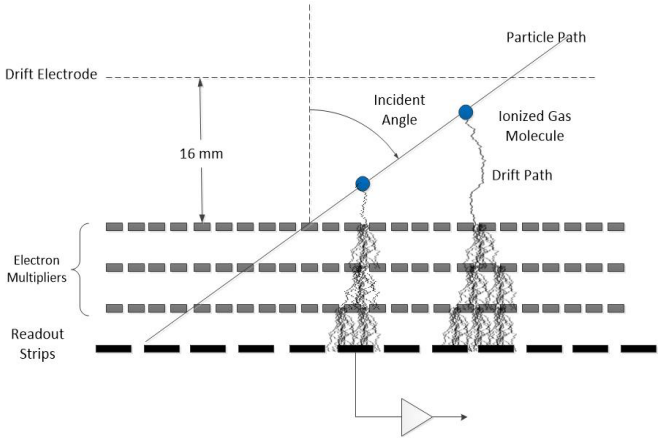

Figure 2. Detection of incoming charged particle [2]

these amplifiers enables determining the location of the input particle's initial ionization.

Because electrons released when ionizing a molecule at the top of a drift region take longer to reach the readout strips than those released at the bottom of the drift region, measuring the time of arrival of electrons at the readout strips as a function of the readout strip location enables measuring the incident angle of the incoming particle. This is illustrated in the diagram of Figure 2, shown with a 16 mm wide drift region. In that figure, the incoming particle has ionized two gas molecules. The electrons released by this ionization drift toward the first GEM electrode due to the impact of an electric field. That GEM electrode multiples the number of electrons moving toward the readout strips and subsequent GEMs further multiply the number of electrons. The time for the resulting shower of electrons to reach the readout strips depends on the distance between the initial ionization location and the top GEM electrode and on the velocity of the electron drift in the drift region. The angle of the incoming particle for this case of the particle ionizing two gas molecules can therefore be determined from the ratio of the vertical distance between the ionizations (computed from the time difference between the 2 readout strip pulse times of arrival multiplied by the drift velocity) divided by the horizontal distance between the readout strips receiving pulses.

Angle-of-Arrival Calculation

In the 2-dimensional example shown in Figure 2, the angle of incidence relative to the normal to the detector is given by $\tan^{-1}(\Delta h/\Delta x)$ where Δh is the difference in height between the first and second ionizations and can be found from the time difference of arrival of the two detections on the readout strips as $\Delta h = v_d \Delta t$ where v_d is the electron drift velocity. For the general 3-dimensional case, refer to Figure 3. The readout strips lie in the x-y plane. We assume the particle arrives along a direction described in polar coordinates by the azimuthal angle ϕ that the track projection onto the x-y plane makes with the x-axis and a the polar angle θ with respect to the z-axis, which is normal to the detector plane. If the incoming particle ionizes a gas molecule at time t_0 at a height h above the array, this ionization will be detected at time $t = t_0 + h/v_d$ on the x readout strip located at $x = p \sin\theta \cos\phi = h \tan\theta \cos\phi$ and on the y readout strip located at $y = h \tan\theta \sin\phi$. As the particle ionizes other molecules along its path, the detection locations on the x and y strips will describe a linear function of time $x(t) = t\ v_d \tan(\theta) \cos(\phi) + x_0$ with slope $s_x = \frac{dx}{dt} = v_d \tan(\theta) \cos(\phi)$ in units of distance per time. The equivalent slope for the y channel is $s_y = v_d \tan(\theta) \sin(\phi)$. This pair of slope equations can easily be solved for θ and ϕ since $\frac{s_y}{s_x} = \frac{\tan(\theta)\sin(\phi)}{\tan(\theta)\cos(\phi)} = \tan(\phi)$ and $\frac{s_y}{v_d \sin(\phi)} = \frac{s_x}{v_d \cos(\phi)} = \tan(\theta)$

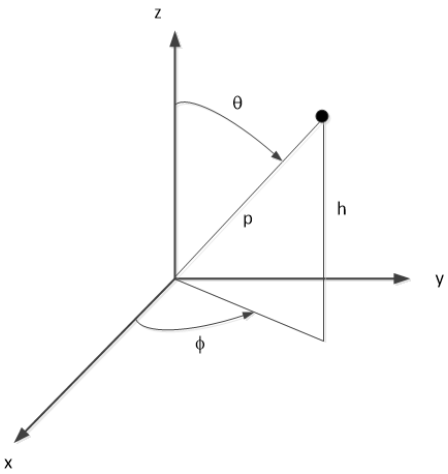

Figure3. 3-d geometry

Thus,

$$\phi = \tan^{-1}\left(\frac{s_y}{s_x}\right) \quad (1)$$

$$\theta = \tan^{-1}\left(\frac{s_y}{v_d \sin(\phi)}\right) = \tan^{-1}\left(\frac{s_x}{v_d \cos(\phi)}\right) \quad (2)$$

Experimental Setup

The remainder of this report is concerned with approaches to compute the slopes from data taken at Fermilab by a group of researchers from Brookhaven National Lab (BNL). The data were taken on a GEM detector with a 16 mm drift region and readout strip pitch of 400 μm using a data acquisition system that sampled the voltage on each strip at a 40 MHz rate [2]. Therefore, converting from the slope measured in channels per sample to a slope in meters per second just requires multiplying by a factor of 400 x 10^{-6}/25 x 10^{-9} =16,000 m/s so that with the drift velocity of 30 mm/μs for the detector used in these experiments, the normalized slope s/v_d used to compute the angle of arrival is simply the slope in channels per sample times 16/30.

Using the MT6 test beam at the Fermilab Test Beam Facility [3] as a source of charged particles, the BNL researchers collected sampled data over a number of particle events with the detector oriented in 5 different positions with respect to the incident beam. In the first three orientations, the detector was aligned so that the beam entered the detector with ϕ = 45° and at incident angles of θ = 45°, 30°, or 15° with θ and ϕ defined as shown in Figure 3. For the 4th orientation, the angle θ was set to 45° and the angle of ϕ was changed to 0° so that the path of the incoming beam aligned with the x-axis readout strips. In the final configuration the incoming beam was aligned with the normal to the plane of the detector. The data for each of these configurations were stored in 5 event files provided by BNL [4], file number 567 for the 45°/45° configuration, file number 569 for the 30°/45° case, file number 589 for the 15°/45° case, file number 511 for the 45°/0° case, and file number 516 for the 0°/0° case. BNL also provided some ROOT code [4] that was used to read these files and using this code we have been able to extract for each incoming particle the pulse amplitude versus sample number on each readout strip. This information was then used as explained above to compute the angle of arrival of the input particle.

Detected Pulse Response to an Incoming Particle

Figure 4 shows an example of the output, sampled at 40 Mega-samples/second, (25 ns/sample) on two different readout strips responding to electrons released by an incoming particle ionizing a pair of molecules in the drift region. This figure, that was computed using data from file 567, demonstrates the difference in the start time of the pulse on different readout strips due to two gas molecules ionized by the same input particle. With just these two figures one can even get a first approximate estimate of the angle θ (assuming we had already found that the angle ϕ was about 45°). The difference in readout strips is 14 and the approximate difference in the start of the pulses is 13 samples so our estimate of θ according to equation (2) is $\tan^{-1}\left(\frac{14}{13}\frac{16}{30}\frac{1}{\sin 45°}\right)$ which evaluates to 39.1° whereas the actual value is 45°.

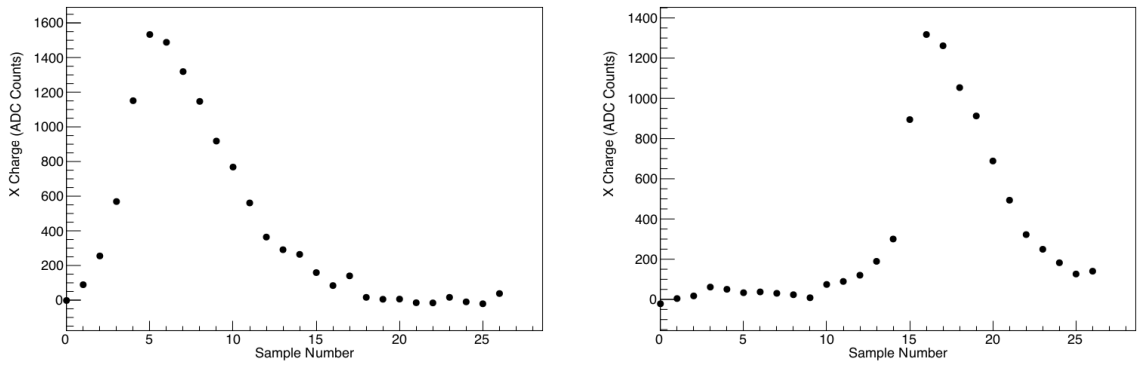

Figure 4. Detector response to incoming particle where each sample corresponds to 25 ns (left plot - readout strip 142; right plot- readout strip 128)

This example highlights a major element necessary to compute the angle of arrival, i.e. the need to detect the presence of a pulse responding to ionization by an incoming particle and to measure the start time of the pulse. Not all pulses due to particles are as well defined as those in Figure 4. Figure 5 is another example of responses to a particle where the time of arrival is not so well defined visually, complicating a general algorithm to measure the start time. It is not clear if the pulse on the left started at sample 10 or at sample 14; however, with the pulse on the right that was measured on the adjacent readout strip the start time is clear. An algorithm that distinguishes between these two cases is difficult to define so that a reasonable approach to measuring the start time is to not attempt to be too discriminating and to allow for the fact that most pulses are reasonably well defined. The larger number of valid pulse measurements will not be significantly impacted by the fewer invalid ones in estimating the slope of channel versus sample.

Visual inspection of a number of these pulse responses revealed that pulse start times are more easily identified on pulses with larger amplitudes. For this reason, the start time was only measured on pulses with a peak amplitude greater than 400 ADC counts.

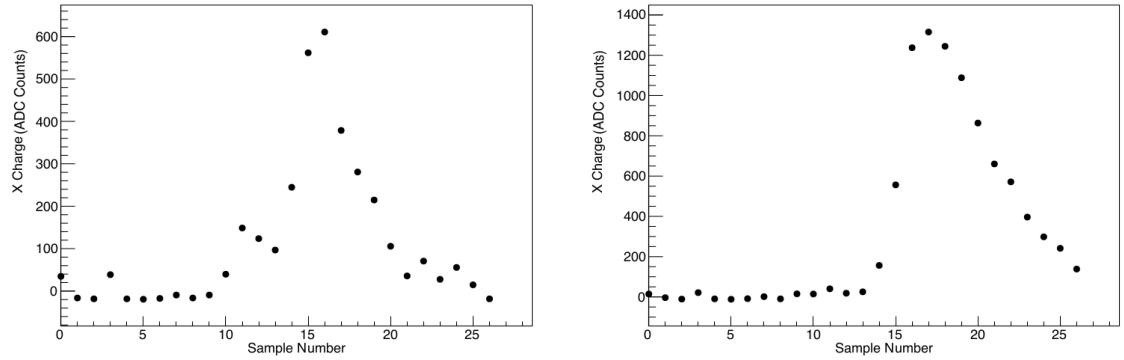

Figure 5. Questionable pulse start time (left plot - readout strip 135; right plot - readout strip 134)

Each input particle ionizes a number of gas molecules as it travels through the drift region so that a number of response pulses are observed for each input particle. To compute the slope of channel versus time it is only necessary to plot the detected responses and to fit a line to the plotted data. Figure 6 is an example of such a plot including a linear fit to the detected responses. The clustering of ionization events along the particle track is quite evident here.

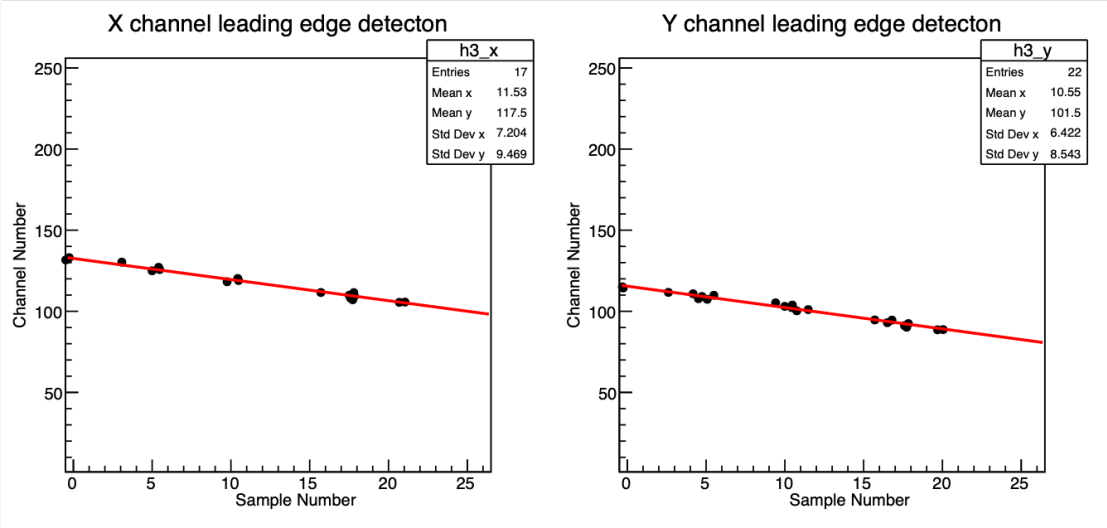

Figure 6. Slope estimation based on detected responses. The ADC sample number reflects the estimated start time of the pulse.

The number of detected clusters used to estimate the slope varies from event to event with an average of a little over 20 clusters per event. Figure 7 histograms the distribution of the number of clusters contributing to a slope estimation for 2000 events in file 567.

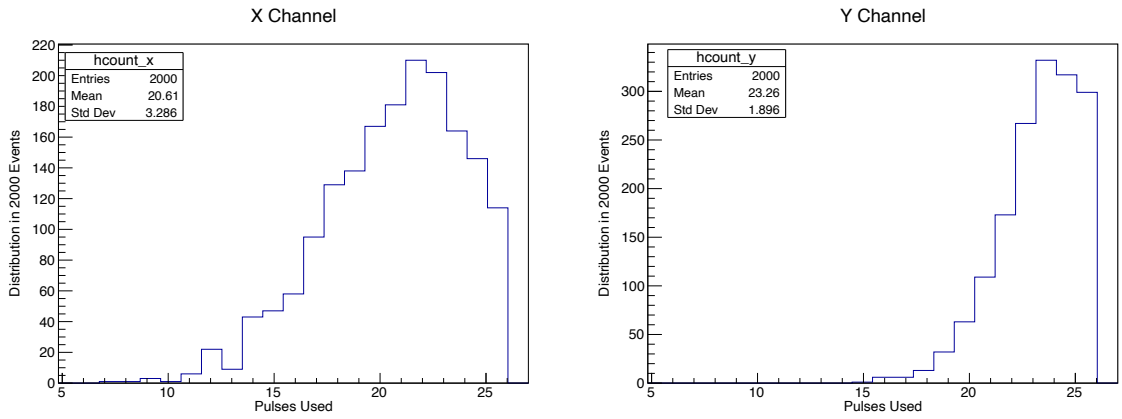

Figure 7. Distribution of detections used in slope estimation

Pulse Time-of-Arrival Estimation Approaches

A number of approaches to measure the TOA of a pulse were investigated. For each approach the AOA of the incoming particle was computed and a histogram of the results was generated. The primary comparison of these approaches was based on data in files 567, 569, and 589 from Fermilab for which ϕ = 45°. As will be discussed later, measuring TOA for the configurations

used in the other two files was not as straightforward. To ensure consistency in the comparison, all calculations used the same set of particle events. As stated earlier, only pulses with a peak value of 400 ADC counts or greater were used.

It should be noted that the resolution results presented here depend on the data measurement hardware. Pulse widths depend on the bandwidth of the electronics used in data collection, and the accuracy of TOA measurments depends on the signal-to-noise ratio of the detector. For this reason these results only indicate the relative performance of different algorithms rather than the absolute resolution achievable independent of the hardware used.

Approach 1: Look for Rapid Increase in Pulse Amplitude (Rising Edge Approach)

The leading edge of pulses sharply rises as seen in Figures 4 and 5. In this approach, the start of the pulse was assumed to be the sample whose next 2 samples exceeded the previous sample by more than 100 ADC counts. Using this approach to determine the TOA, the values of θ and ϕ were computed using equations (1) and (2) for 2000 events in file 567. Histograms of the results are shown in Figure 8 along with a Gaussian fit to the histogram for the purpose of estimating the resolution of the estimate.

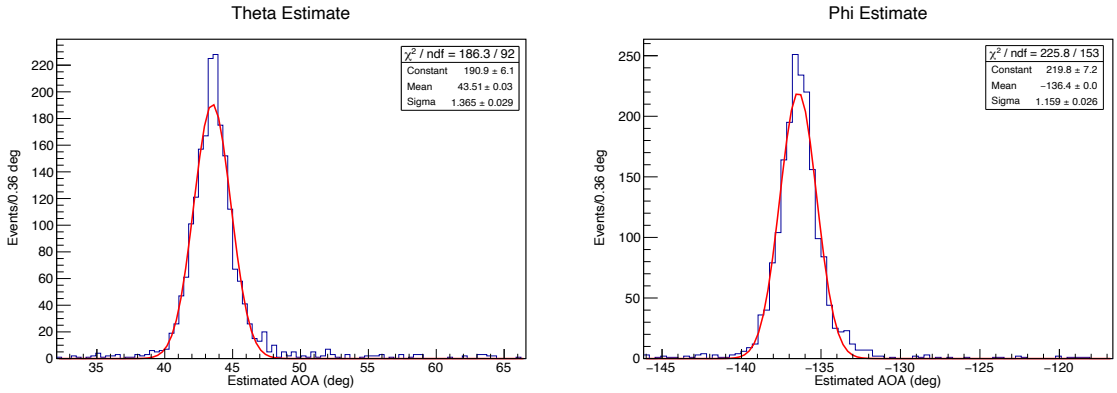

Figure 8. Estimated AOA using rising edge

The estimated angles of arrival are clustered about a mean with an RMS error of around 1° to 1.5°. In addition to this random fluctuation there is a mean offset in the result of about 1.5° in θ and 1.4° in ϕ from the assumed true DOA. The reason for this offset is unknown. It could possibly be due in part to a misalignment of the detector in the setup with respect to the desired alignment. It could also be due to an error in the assumed drift velocity of electrons in the drift region, although the computation of ϕ should be independent of drift velocity as indicated in equation (1).

Approach 2: Best Linear Fit to Leading Edge (Slope Intercept)

A disadvantage of the Rising Edge approach is that the TOA is restricted to one of the samples and it cannot account for how fast the leading edge rises. This quantization of TOA may have the effect of increasing the variation of the results.

To possibly mitigate these potential deficiencies, a linear fit to the leading edge was tried with the TOA specified to be the time that this linear fit intersected with the horizontal axis. This approach, called slope intercept in this report, appears to be essentially the same approach as

one that the BNL researchers called rising edge [5]. (Note: This is not to be confused with Approach 1, which is also called rising edge.) A number of ways to specify the samples used for the leading edge fit of the pulse were tried. The approach that restricted the leading edge to the sample with the maximum value and the 2 previous samples worked best. Another approach using the ROOT Fit function to fit a line to the leading edge would fail when the main part of the pulse was preceded by a slowly rising output. In these cases, the fit function would choose the slowly rising portion of the pulse which would result in an early estimation of pulse TOA. A particularly egregious example of this type of failure is shown in Figure 9. Even initializing the fit function to more closely approximate the true leading edge did not change the fit result. Since all pulses that exceeded the 400 ADC count minimum pulse height had at least 3 samples on the leading edge, the most straightforward way to ensure not including these slow rises in the estimation was to restrict the samples used to the maximum sample and the 2 prior ones.

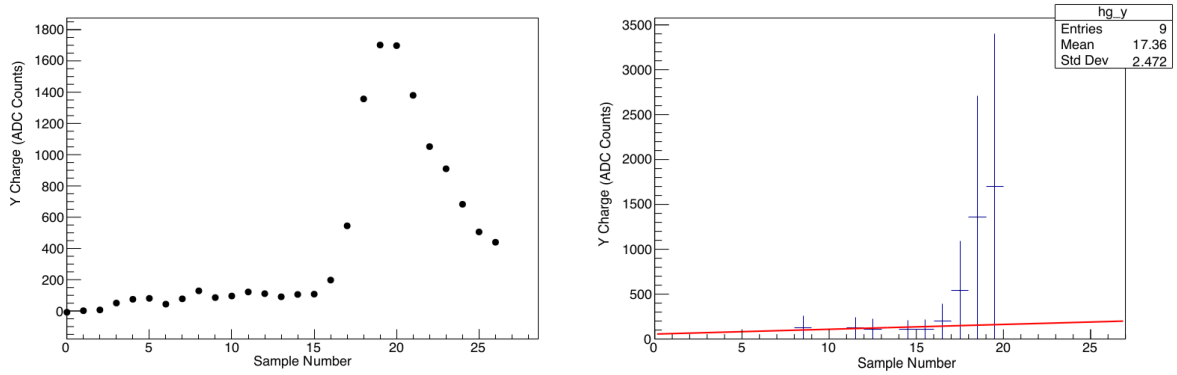

Figure 9. A problem finding the pulse leading edge with a fit of the leading edge

Using this leading-edge slope intercept algorithm with the leading edge restricted to 3 samples, the AOA was again computed for the same set of 2000 particle events. The results computed using this algorithm are shown in Figure 10, along with a double-Gaussian fit to these results. The amplitudes of the core and secondary Gaussian fit are given by p0 and p3. The mean of the fit is p1 and the standard deviation of the core and secondary fits are p2 and p4. Comparison of these results with those of Figure 8 shows roughly the same performance. The resolution in θ is better with the slope intercept than with the rising edge, although the offset of the mean from the nominal value of 45° is higher. The resolution in ϕ is slightly worse, although the difference is possibly within measurement error as indicated by their respective estimation errors.

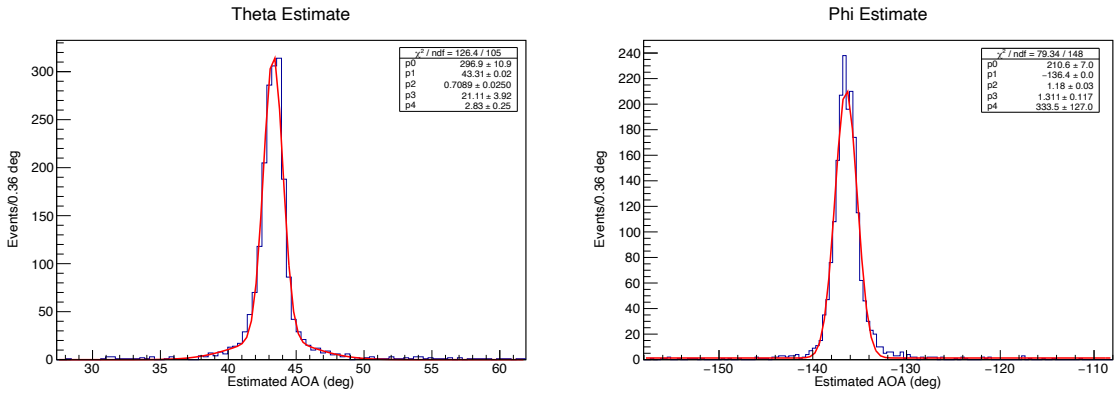

Figure 10. Estimated AOA using slope intercept

Approach 3: Fit a Function to the Pulse (Landau Fit)

The shape of detector pulses is determined to a reasonable degree by the amplifier electronics connected to the readout strips. Rather than attempt to identify the start of a pulse, another approach to determining the pulse time of arrival is to fit a variable start time function approximating the shape of a pulse to the detector data and then to read the value of the fit start time.

One such function approximating the pulse shape is

$$f_2(t) = ae^{-(e^{-b(t-\tau)}+b(t-\tau))/2)}.$$

This function [6], whose shape approximates a Landau function, not only includes a variable start time variable, but it includes a variable time scale factor b which enables better fitting to data with variable pulse widths. For each pulse with a maximum value greater than 400 ADC counts, the data were fitted to this function using the ROOT Fit function. The fitted value of τ was then used as the pulse start time. Although τ is not really the start time of the pulse (it is the time the pulse reaches its maximum value), to the degree that the scale factor b doesn't change, τ just differs from the start time by a constant value. Since there will be some variation in the detected pulse widths, the factor b is not constant and this will cause some small variation in the measured TOA. A more complicated algorithm could possibly account for some of this variation in the TOA, but an attempt to find such an alternative was not made. Figure 11 illustrates the fitting of this function to the pulse output of 3 different readout strips responding to the same input particle. This sequence of figures illustrates how the fit is able to extract the pulse position over a variety of pulse shapes. The examples for channels 141 and 130 were selected because they illustrate fitting to an atypical pulse shape. Usually the pulse shape was more like that of the leftmost plot, channel 152.

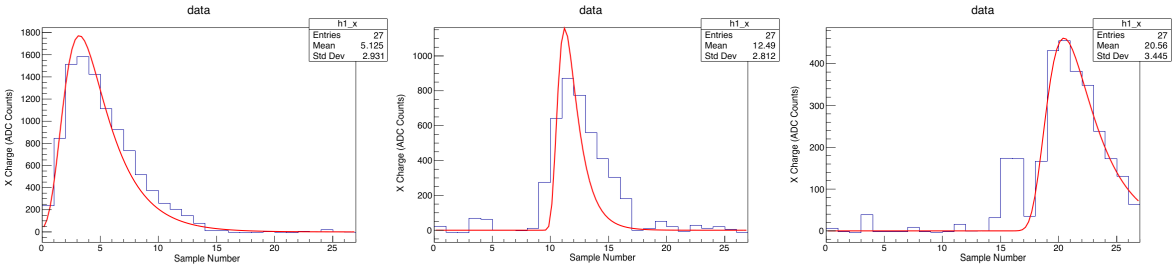

Figure 11. Landau fit to pulses (left plot - chan 152; middle plot - chan 141; right plot - chan 130)

A histogram of the AOA estimation results using this Landau fit approach is shown below in Figure 12. This result, when compared with the result using the slope intercept method, indicates a clear improvement with respect to the RMS error, although the discrepancy of the mean from the assumed true values (45°/45°) is slightly greater in both the θ and the ϕ directions.

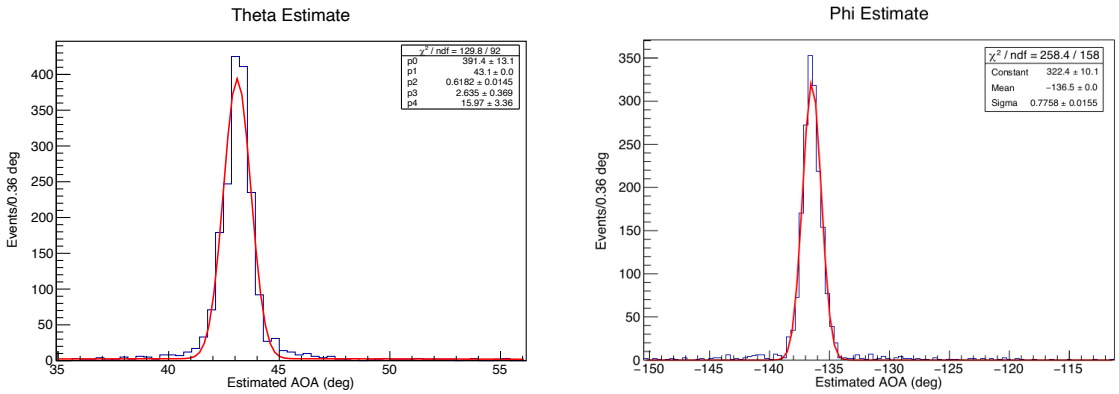

Figure 12. Estimated AOA using Landau fit

As the angle of incidence of the incoming beam is reduced, the distance between ionizations in the drift region as projected on the plane of the detector also reduces. This can cause the detected pulses to tend to overlap, possibly impacting the measurement accuracy of the algorithms. The data in files 569 and 589 with angles of incidence of 30° and 15° respectively were processed to investigate the impact of angle of incidence on AOA accuracy.

Figure 13 shows the AOA computed for the data in file 569 when using the slope intercept algorithm and Figure 14 shows the results for the Landau fit algorithm.

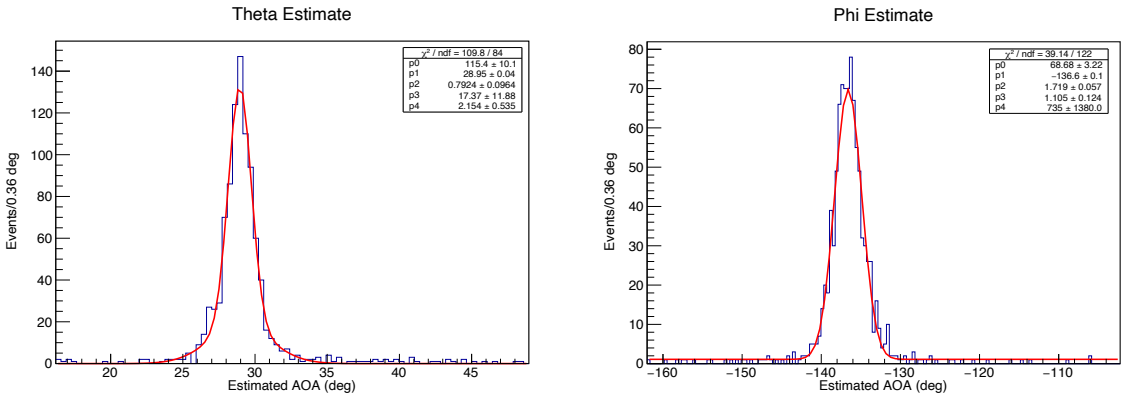

Figure 13. Estimated AOA using slope intercept for 30° incidence angle

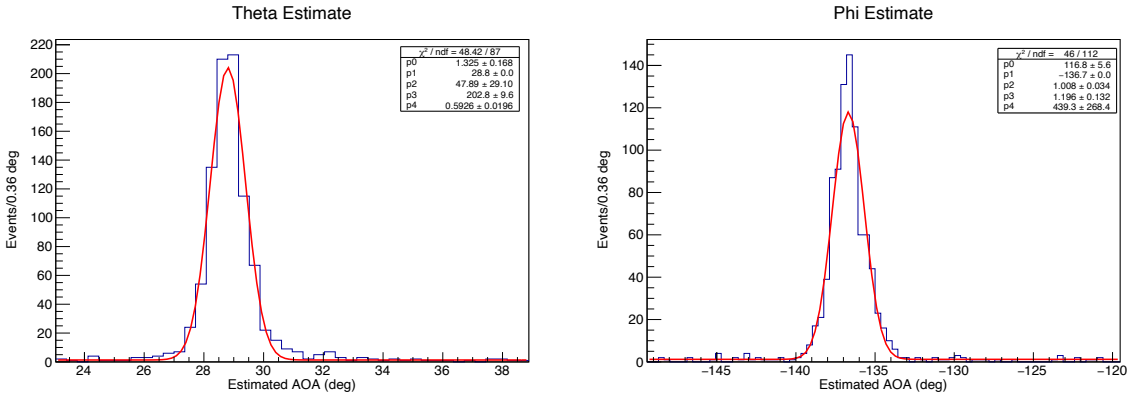

Figure 14. Estimated AOA using Landau fit for 30° incidence angle

Inspection of these figures verifies that the Landau fit algorithm is still superior to the slope intercept algorithm and that reducing the angle of incidence to 30° from 45° mostly had an impact on the angular resolution of phi when using the slope intercept algorithm.

The equivalent results obtained when processing file 589 for 15° incidence angle are shown in Figures 15 and 16.

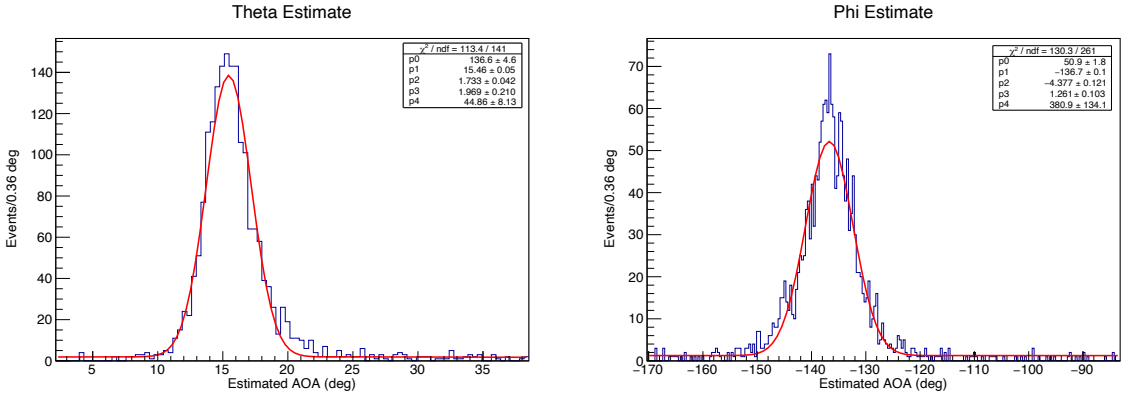

Figure 15. Estimated AOA using slope intercept for 15° incidence angle

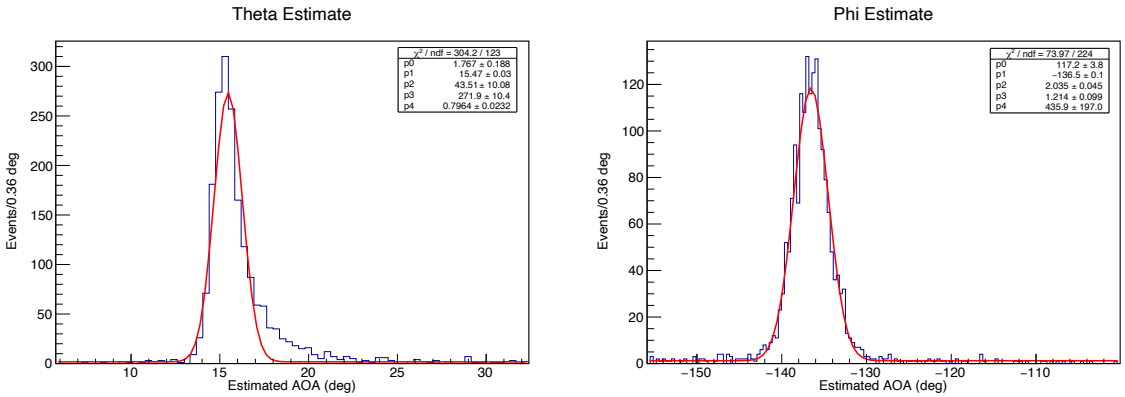

Figure 16. Estimated AOA using Landau fit for 15° incidence angle

In these figures one can see the degradation in the AOA resolution estimates due to a small beam angle of incidence when using either the slope intercept algorithm or the Landau fit algorithm. In addition, although with the estimation of θ the core of the estimated angle distribution is reasonably fitted with a Gaussian function, there is also a large asymmetric tail to the distribution. These large tails are likely due to a bias imposed by cross-talk [7].

Algorithm Failures

For most events, the algorithm for measuring the TOA of a pulse worked well and the calculation results of θ and ϕ are reasonably well clustered about a mean value. There are, however, some results that are scattered over a large range of angles. These cases are not immediately visible in the histograms of Figures 8, 10, and 12, because there are only 1 or 2 values for any specific angle. In Figure 17 the axis has been zoomed to illustrate the number of results with large offsets from nominal.

Some specific events that resulted in large offsets were identified and the data for these events were investigated. Figure 18 shows plots of data for the x-channel for two events resulting in large offsets. Data for the y-channel looked similar. Rather than the ionization from a single particle being detected, the result looks as though many particles arrived simultaneously. It is not known for certain that this is actually due to an input with many simultaneous particles rather than due to some problem with the data acquisition hardware or software. In Figure 19 one can see tracks corresponding to the left plot of Figure 18. The tracks from multiple particles make nearly the same angle with the readout strip. But since the processing algorithm expected only a single linear track of detections, it failed to find a reasonable linear fit to the data as indicated by the red fit line. If multiple simultaneous particle arrivals are expected to be a common occurrence for the naturally occurring particles whose AOA is to be measured, a means of identifying and ignoring these events will need to be developed.

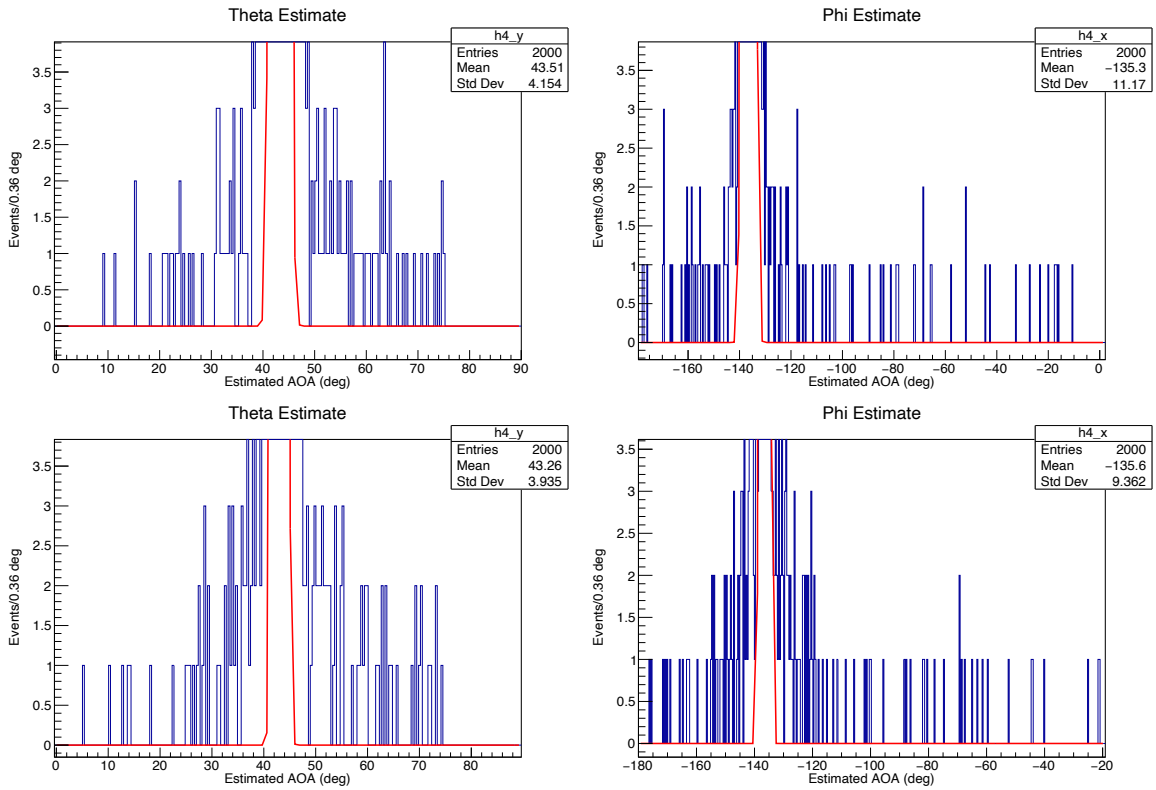

Figure 17. Large angle offset results (top row - slope intercept, bottom row - Landau fit)

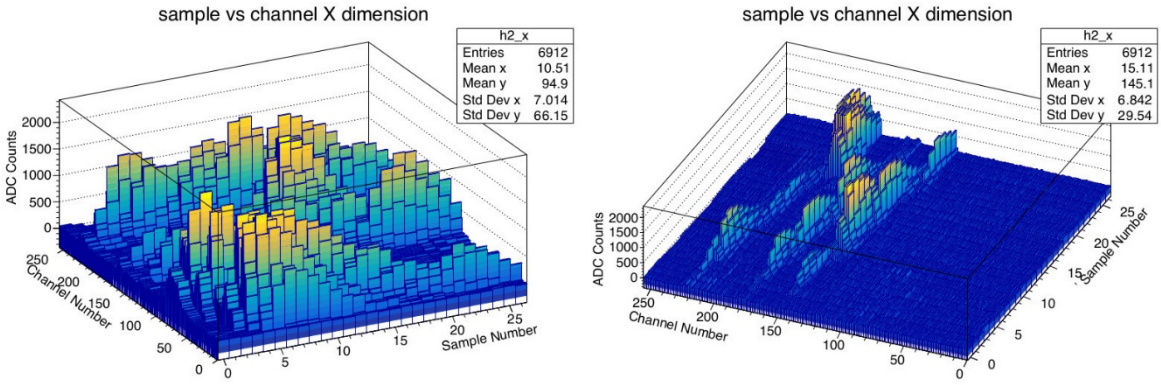

Figure 18. Two example events with large discrepancies

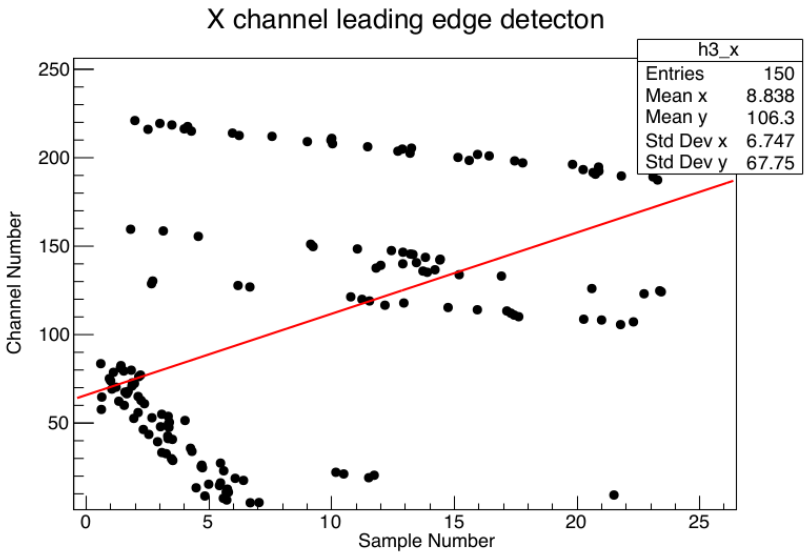

Figure 19. Detections resulting from multiple particles of figure 14 (left panel)

Angle Deviation from Nominal

The variation in estimation of the AOA is a combination of variations in θ and ϕ. One approach to combining these variations is to average them in quadrature. When this is done an approximation to an equivalent angular resolution is

$$\sigma = \sqrt{\left(\sigma^2{}_\theta + \sigma^2{}_\phi \sin^2\theta\right)/2}. \quad (3)$$

The factor of $\sin^2\theta$ on the variance of ϕ accounts for the fact that the angular standard deviation in the direction normal to θ is $\sin\theta\,\sigma_\phi$. An alternative measure of AOA resolution is to fit a Rice probability density [8] to a histogram of angular deviation computed by taking the dot product of the assumed nominal AOA with the measured AOA.

The Rice probability density is defined as

$$p(r) = \frac{r}{\sigma^2} e^{-\frac{r^2+\mu^2}{2\sigma^2}} I_0\left(\frac{r\mu}{\sigma^2}\right), \quad (4)$$

where $I_0(\cdot)$ is the modified Bessel function of the first kind of order 0. This function is exact when the AOA variation is made up of a pair of orthogonal Normal random variables each with standard deviation σ and with a mean $\mu = \sqrt{\mu_1{}^2 + \mu_2{}^2}$ where μ_1 and μ_2 are the means of the respective variables. Fitting a Rice density function will provide another equivalent estimate of the AOA resolution with the advantage that it provides a single probability measure that includes the impact of mean offsets from nominal. The histograms of the measured AOA relative to the assumed nominal AOA for each TOA algorithm are shown in Figure 20 along with a fitted Rice density function. Each figure also shows the values μ and σ for the density fitted to the histogram of measured values.

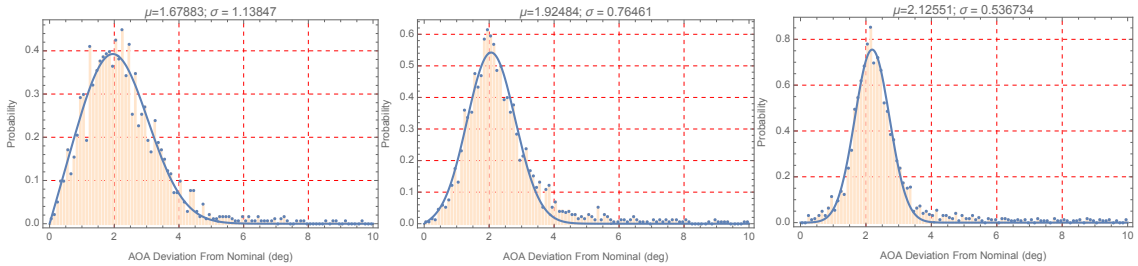

Figure 20. AOA deviation from normal (left plot- rising edge; middle plot - slope intercept; right plot - Landau fit)

A summary of the results computed using different TOA algorithms for data from the three files for which ϕ equals 45°, is shown in table 1 below. The equivalent angular resolution computed by combining the θ and ϕ resolutions according to equation (3) is compared with the Rice function fit to the measured total resolution. There is good agreement between the two estimates of resolution. The columns headed $|\Delta\mu_\theta|$ and $|\Delta\mu_\phi|$ are the absolute values of the difference between the assumed nominal θ and ϕ angles and the mean value of the measured angles.

Table 1. AOA resolution computed for 3 measurement approaches with ϕ = 45°

Algorithm	$\boldsymbol{\theta}$ **(deg)**	$\boldsymbol{\sigma_\theta}$ **(deg)**	$\boldsymbol{\sigma_\phi}$ **(deg)**	$\boldsymbol{\lvert\Delta\mu_\theta\rvert}$ **(deg)**	$\boldsymbol{\lvert\Delta\mu_\phi\rvert}$ **(deg)**	$\sqrt{(\sigma^2{}_\theta + \sigma^2{}_\phi \sin^2\theta)/2}$ **(deg)**	**Rice Fit (deg)**
Rising Edge	45	1.37	1.16	1.5	1.4	1.13	1.14
Slope Intercept	45	0.71	1.18	1.7	1.4	0.77	0.76
	30	0.79	1.72	1.0	1.6	0.83	.92
	15	1.7	4.4	0.5	1.7	1.45	1.45
Landau Fit	45	.62	0.78	1.9	1.5	0.57	0.54
	30	.59	1.0	1.2	1.7	0.55	.53
	15	.80	2.0	0.5	1.5	0.67	.77

Comparison with BNL Results

The BNL results published in the paper of reference [2] were primarily concerned with estimating the position and angle of the beam track to improve the position resolution of the detector, particularly at large incident angles. Because of this the authors did not provide resolution results for angle of arrival. Their results provided a resolution of the beam track as measured on the individual x and y readout strips along with an equivalent resolution calculated by combining the individual readout strip resolutions in quadrature. This section provides our equivalent to those results for computations using the slope intercept and Landau fit algorithms and compares these results to the results that BNL presented for their rising edge

algorithm. That algorithm is similar to, if not identical to, the slope intercept algorithm described above.

The BNL results quoted here were read off figure 15 in the BNL paper (reference [2]). That figure plots the computed angular resolution as a function of angle of incidence, but, as best as we can understand, the angle of incidence shown in this figure is not the same as the angle of incidence relative to the normal to the detector plane, but is the angle projected on the x-z or y-z plane. For this reason, the angles of incidence for ϕ of 45° and θ of 45°, 30°, and 15° will become 35.3°, 22.2°, and 10.7° respectively. Measurement points for angles of incidence very near these values are plotted in figure 15 of the BNL paper.

To directly compare these results with those of BNL, a histogram of the beam track resolution for the x and y axes was computed. The slope resolutions measured with these histograms are shown in Table 2 below. This direct measurement of the angular resolution reported by BNL shows the slope-intercept algorithm resolution equal to, or worse than, that reported by BNL for their rising edge algorithm and the Landau fit resolution 10-20% better than the BNL result.

Table 2 Comparison with rising edge BNL slope measurements

Algorithm	**θ (deg)**	**Angle of Incidence (deg)**	**σ_x (deg)**	**σ_y (deg)**	**$\sqrt{(\sigma_x^2+\sigma_y^2)/2}$ (deg)**	
			These Results	**These Results**	**These Results**	**BNL Results**
Slope Intercept	45	35.3	.79	.76	.78	.74
	30	22.2	.97	.77	.88	.69
	15	10.7	1.56	1.30	1.44	.92
Landau Fit	45	35.3	.69	.65	.67	.74
	30	22.2	.56	.59	.58	.69
	15	10.7	.68	.73	.71	.92

Although our results showed that with the slope intercept algorithm (equivalent to the BNL rising edge algorithm), reducing the angle of incidence of the particle beam monotonically degraded the angular resolution, BNL detected an initial improvement in resolution as the incidence angle reduced, until eventually degrading with a further reduction in angle of incidence. The reason for this difference is not known, although the difference could be due to BNL using a better pulse TOA determination algorithm than our slope intercept algorithm or that BNL processing possibly accounted for variable detector baseline and noise, which was not done with our processing. When the beam angle of incidence was large, our results coincided with those of BNL.

Our results, obtained when using the Landau fit to estimate pulse TOA, exhibited the same initial improvement in resolution with reduction of the angle of incidence as did BNL. In

addition, the Landau fit algorithm resulted in better resolution estimates than were reported by BNL.

The Concern When the Beam Path is Aligned with a Readout Strip

The experimental data from two additional beam directions with respect to the detector orientation were also evaluated. In the data of file 516, the incoming beam was normal to the plane of the detector array. In the data of file 511, the incoming beam was aligned with the x readout strip. The relatively poor resolution resulting from this beam alignment is discussed in this section.

File 511 data was taken with ϕ = 0° where the input beam is aligned with the x readout strips so that ideally all pulses would fall on only a single x-readout strip. There are a total of 5 cases that result in the input particle path aligning with either the x or y readout strips. These angles are when ϕ is at either 0°, 90°, 180°, or 270° and when θ is 0°. In the normal beam case the particle path aligns with both the x and y strips.

If the individual pulses in these cases were identifiable, then small angles would not cause a problem in measuring pulse TOA. But when the beam aligns with a readout strip, most pulses will overlap preventing measurement of TOA. An example of this is shown in Figure 21 below. On the y-readout strips, that make an angle with the incoming particle path, multiple pulses are detected as shown in the rightmost two plots in that figure, verifying that multiple discernable ionizations occurred in the drift gap. But on x-readout strip 162, as seen in the leftmost plot, all the pulses resulting from multiple ionizations overlap, destroying the ability to measure pulse TOA.

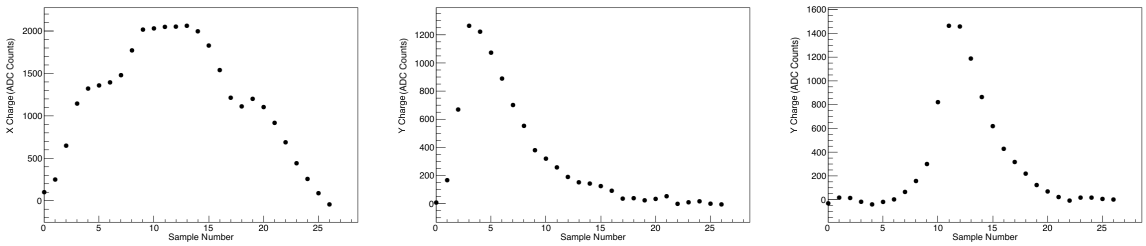

Figure 21. Readout strip voltages with ϕ=0 (left plot - x strip 162; middle plot - y strip 130; right plot - y strip 115)

In some cases, the incoming particle ionizes only a small number of gas molecules so that an individual pulse can be recognized, at least when using a Landau fit to find the pulse. An example of this is shown in the leftmost plot of Figure 22. Visually, it appears that there were at least 3 pulses on this particular readout strip. The Landau fit picked out the strong pulse that peaks at sample 12. When enough pulses can be reliably detected to develop a slope as shown in the rightmost plot in Figure 22, an AOA can be computed. Unfortunately, since the slope must be determined from so few pulse detections, this leads to potentially large errors in the estimation of AOA.

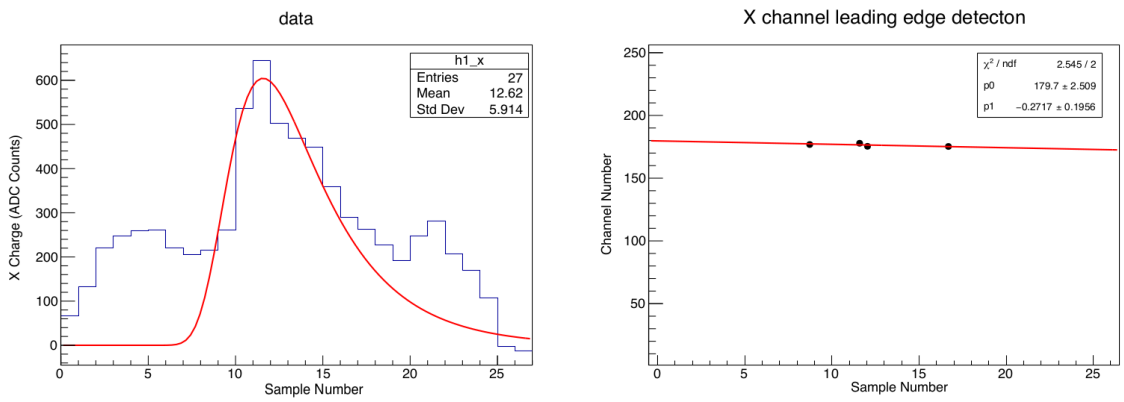

Figure 22. Small angle impact on estimation of ϕ (left plot - detected pulse; right plot - slope estimation)

The estimation errors of θ and ϕ for the Landau fit to the data of file 511 are shown in Figure 23. In Table 3 comparing these results with those of Figure 12, we find only a small impact on the standard deviation of the estimation for the angle θ but a significant impact for the angle ϕ. The reason for this is that according to equation (3) the angle θ can depend on the y channel slope when ϕ is small and the cosine function of ϕ is relatively insensitive to variations in ϕ.

Table 3. Impact of small angle on AOA measurement results

Figure	$\boldsymbol{\sigma_\theta}$ **(deg)**	$\boldsymbol{\sigma_\phi}$ **(deg)**	$\boldsymbol{\lvert\Delta\mu_\theta\rvert}$ **(deg)**	$\boldsymbol{\lvert\Delta\mu_\phi\rvert}$ **(deg)**	$\boldsymbol{\sqrt{(\sigma_\theta^2+\sigma_\phi^2/2)/2}}$ **(deg)**	**Rice Fit** $\boldsymbol{\sigma}$ **(deg)**
12 (ϕ = 45°)	.62	.78	1.9	1.5	.57	.54
23 (ϕ = 0°)	.74	3.59	1.4	6.3	1.87	2.22

When the input path is normal to the plane of the detector, both the x and y readout strips make a small angle with the input path. In this case the estimation of θ would be expected to be significantly impacted. The rightmost panel in Figure 23 shows the estimation of θ in this case. For a path normal to the detector plane, the angle ϕ has little meaning with respect to AOA resolution, so this histogram is not shown. Although the estimated error is clustered near the actual value of 0°, the estimates are distributed over a wide range of value. Thus, even using the Landau fit to individual pulses is not a reliable way to estimate AOA in this case.

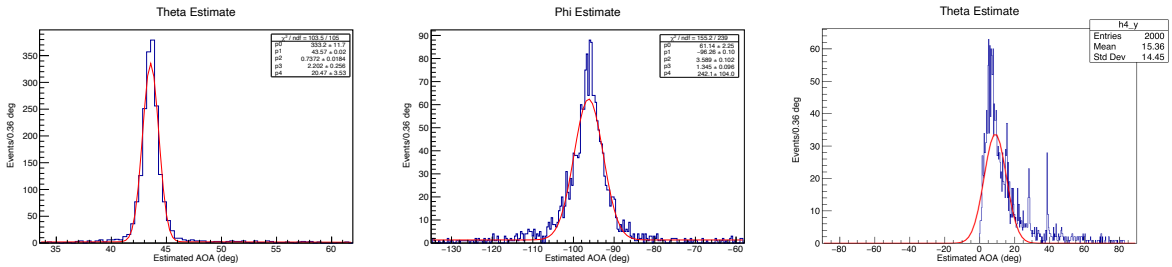

Figure 23. AOA estimate with Landau fit for small track angles (left & middle plots - beam aligned with x-readout strips; right plot - normal beam)

Time Slice Approach

To enable estimation for these small angles the BNL researchers used what they called a time slice approach [2]. In this approach, rather than attempt to measure the TOA of pulses on each readout strip they measured the centroid of charge (amplifier output) over the readout strips for each time sample. The slope was then, as before, a linear fit to the plot of centroid vs. sample. Accurate measurement of the centroid of the charge over the readout strips is key to accurately estimating AOA.

Since only an approach that does not rely on measuring pulse TOA has a chance of providing satisfactory AOA performance at small angles, we looked at a few simple time slice type algorithms that do not require accurately estimating the baseline. The first approach was to directly measure the charge centroid by computing the mean value of the readout strips weighted by the charge on that strip as long as the charge exceeded 100 ADC counts. The second approach was to simply assume the strip with the maximum value is the centroid, similar to what the BNL researchers called the “digital method” in [2]. A third approach involved computing a Gaussian fit to the charge vs. readout strip and using the mean value of the fit as the centroid estimate.

Figures 24 through 26 show the AOA results for the time slice method when using the Gaussian fit to estimate the centroid of the charge. As mentioned earlier, for a normal incidence incoming particle, ϕ is not a useful measure.

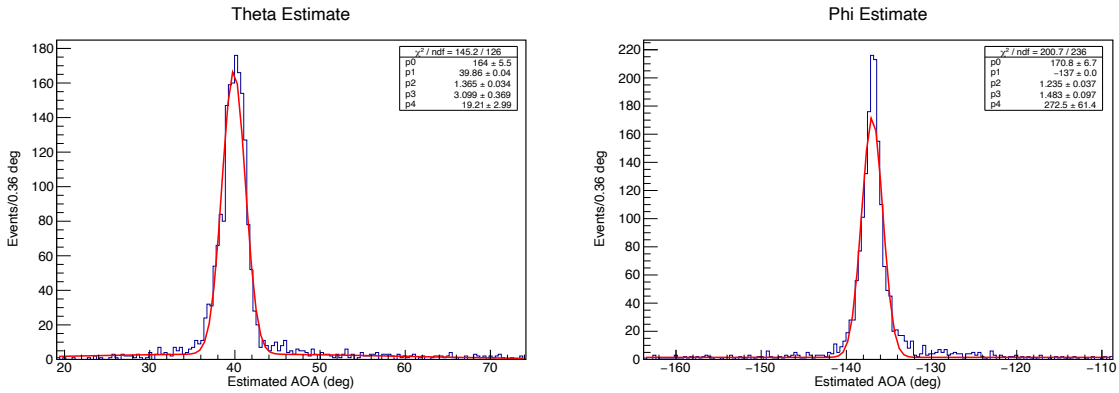

Figure 24. AOA results with time slice fit (θ = 45°, ϕ = 45°)

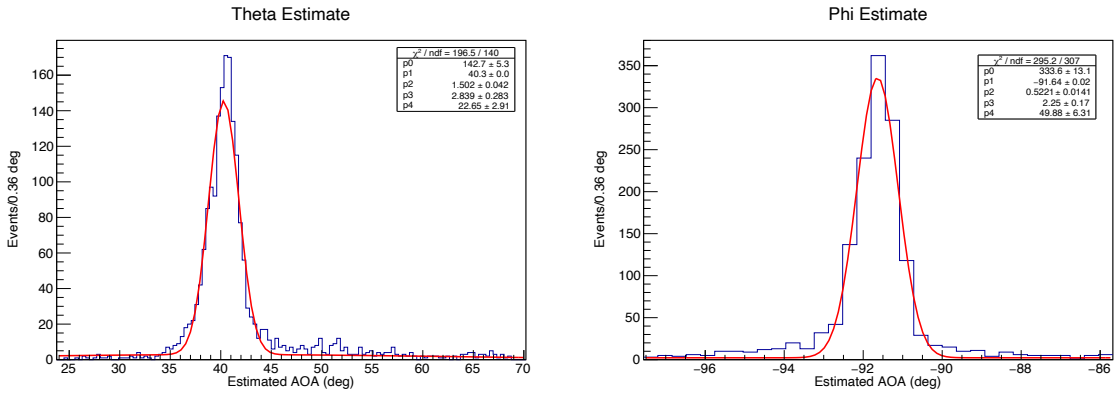

Figure 25. AOA results with time slice fit (θ = 45°, ϕ = 0°)

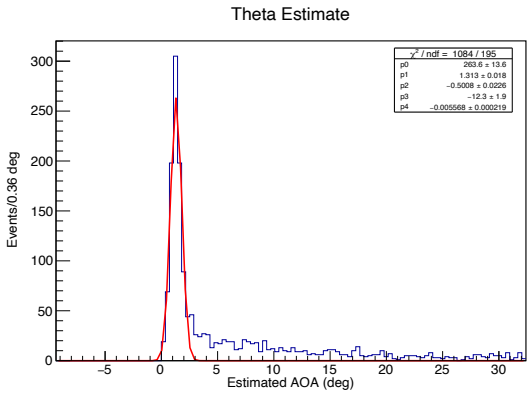

Figure 26. AOA results with time slice fit (θ = 0°)

The equivalent plots when the readout strip with the maximum charge is assumed to be the centroid of charge are shown in Figures 27 through 29.

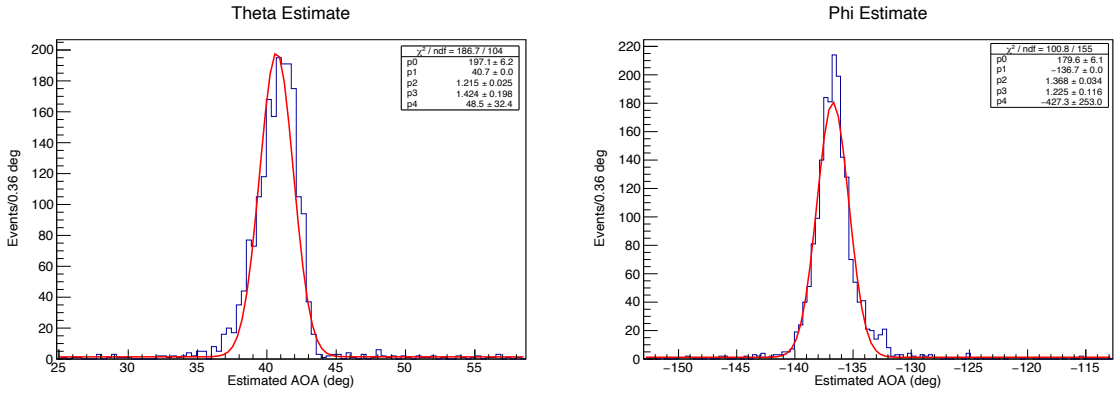

Figure 27. AOA results with time slice max (θ = 45°, ϕ = 45°)

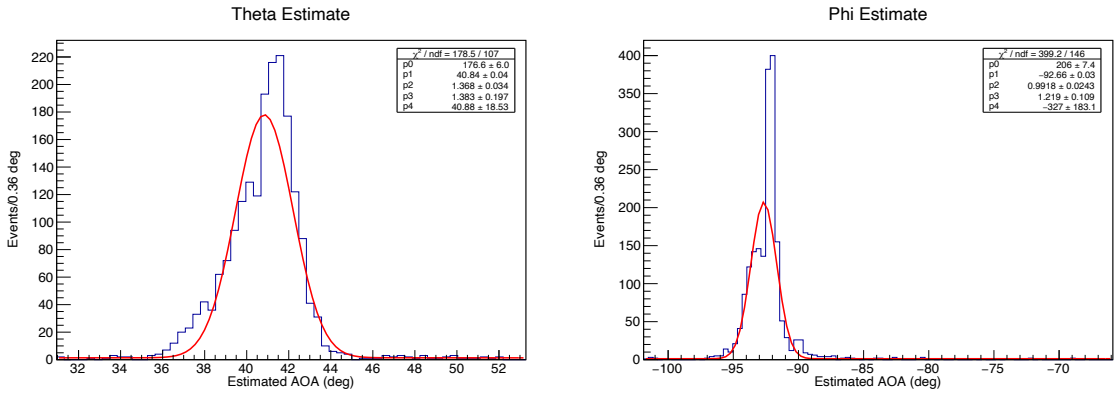

Figure 28. AOA results with time slice max (θ = 45°, ϕ = 0°)

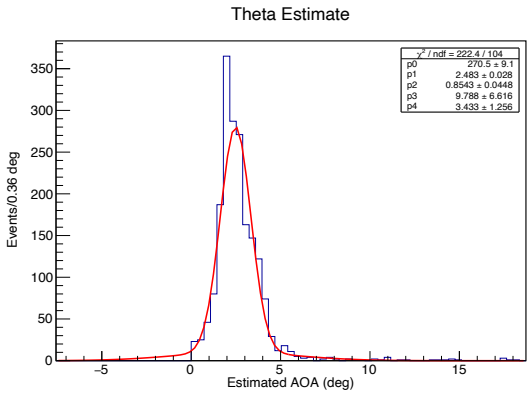

Figure 29. AOA results with time slice max (θ = 0°)

The plots of Figures 30 through 32 show the equivalent results when the centroid is calculated as the average of the charge weighted readout strip.

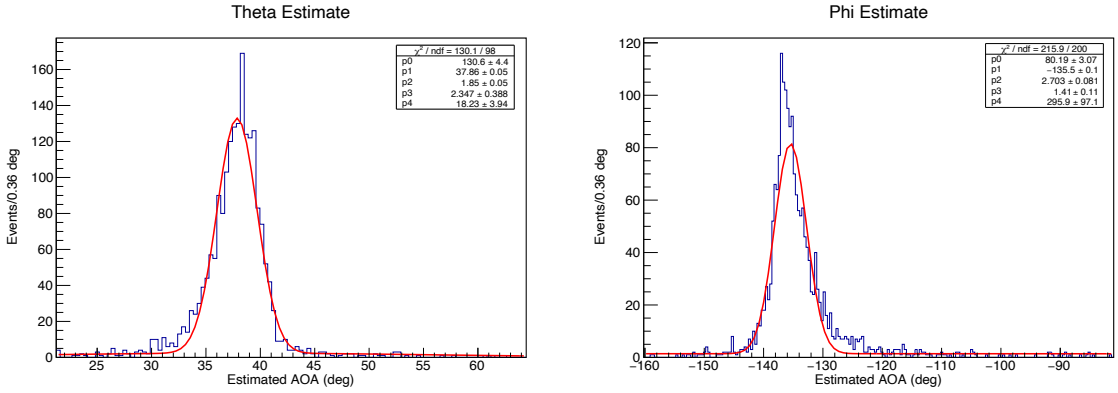

Figure 30. AOA results with time slice calculated centroid (θ = 45°, ϕ = 45°)

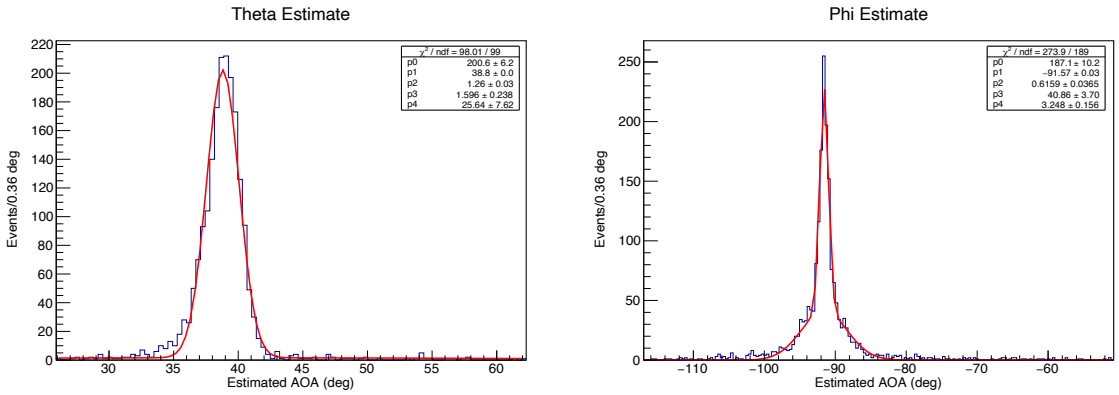

Figure 31. AOA results with time slice calculated centroid ($\theta = 45°$, $\phi = 0°$)

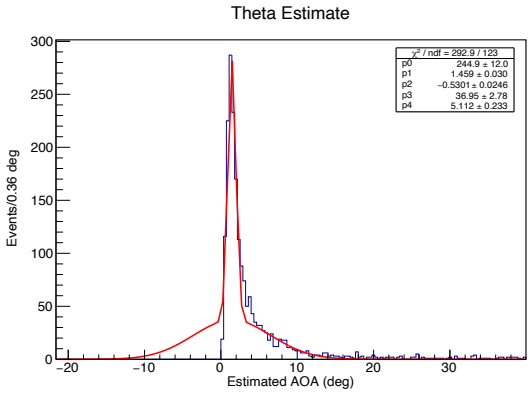

Figure 32. AOA results with time slice calculated centroid ($\theta = 0°$)

Although the time slice method did enable measuring AOA even when the input beam was normal to the plane of the array, two factors in these results may limit their usefulness. First is the large error tail in θ, particularly in the case of the normal beam with calculated centroid. Also, in almost all cases, the estimated mean of the main error distribution was significantly larger for the time slice approaches than for the pulse TOA approaches. Table 4 summarizes the results from Figures 24 through 32.

Table 4. Summary of time slice approximation results

Algorithm	θ/ϕ **(deg)**	σ_θ **(deg)**	σ_ϕ **(deg)**	$\lvert\Delta\mu_\theta\rvert$ **(deg)**	$\lvert\Delta\mu_\phi\rvert$ **(deg)**	$\sqrt{(\sigma^2{}_\theta + \sigma^2{}_\phi \sin^2\theta)/2}$ **(deg)**	**Rice Fit (deg)**
Gaussian Fit	45/45	1.37	1.24	5.1	2.0	1.15	1.29
	45/0	1.50	.52	4.7	1.6	1.09	1.46
	0/0	.50	---	1.31	---	---	.43
Max Charge	45/45	1.22	1.37	4.3	1.7	1.10	1.29
	45/0	1.37	.99	4.2	.99	1.09	1.33
	0/0	.85	---	2.48	---	---	.87
Calculated Centroid	45/45	1.85	2.7	7.1	1.50	1.88	1.61
	45/0	1.26	.62	6.2	1.57	.94	1.36
	0/0	.53	---	1.50	---	---	2.07

Although, as anticipated, these simple approximations to compute a charge centroid do not provide as accurate an estimate of AOA as the TOA based algorithms, most of the estimates are not dramatically offset from the nominal value. Comparing the results in Table 4 above, one concludes that just using the readout strip with the maximum charge at each sample time is as acceptable an approach to simple time slice processing as attempting a Gaussian fit to the charge as a function of readout channel. Computing the centroid by charge weighted averaging of the readout strip resulted in slightly degraded results compared to the other approaches. This was likely due to using a fixed charge threshold to limit the readout strips averaged. An adaptive threshold as was possibly used by BNL would most likely provide improved performance.

Although, for particle beams that did not align with a readout strip, none of these approaches provided angular resolutions better than those of the TOA measurement approaches. At least the time slice provides a reliable measurement approach when the beam aligns with a readout strip.

Considerations for Follow-on Work

Based on the calculations described above on data taken by BNL, it appears that AOA estimations on the order of 0.5° to 1° are possible. An attempt to experimentally confirm this using locally available hardware is in the planning stages. This section outlines a challenge with respect to the width of the drift gap in the detector. The BNL minidrift detector had a drift gap that was 16 mm wide, but a detector available for local testing has only a 3 mm wide drift gap. The impact that a small drift gap will have on the expected performance is examined below.

Impact of Drift Gap Width

It was expected that using a lab detector with a 3 mm drift gap would have a significant impact on the AOA resolution of the detector. To investigate the potential resolution using the lab detector, a lab detector was emulated by processing only ionizations from the lower 3 mm of the minidrift detector. This was done by only estimating the channel vs. sample slopes using BNL data pulse start times occurring in the first 5 samples. An example of the estimates of the AOA is given in Figure 33 below. The angle estimates in this figure used the BNL data corresponding to θ of 45° and ϕ of 45° with the pulse TOA computed using the Landau fit algorithm. Comparing the results of this figure with those of Figure 12, the angular resolution in Figure 33 is about 12 degrees in θ and 6 degrees in ϕ, as opposed to the equivalent values of 0.6 degrees and 0.8 degrees for a 16 mm drift gap shown in Figure 12. This illustrates the significant impact of reducing the drift gap to 3 mm. Not only has the resolution significantly degraded, particularly in the estimate of θ, but a spurious result at an estimated AOA of 90° has appeared both in θ and ϕ; it is most noticeable in θ.

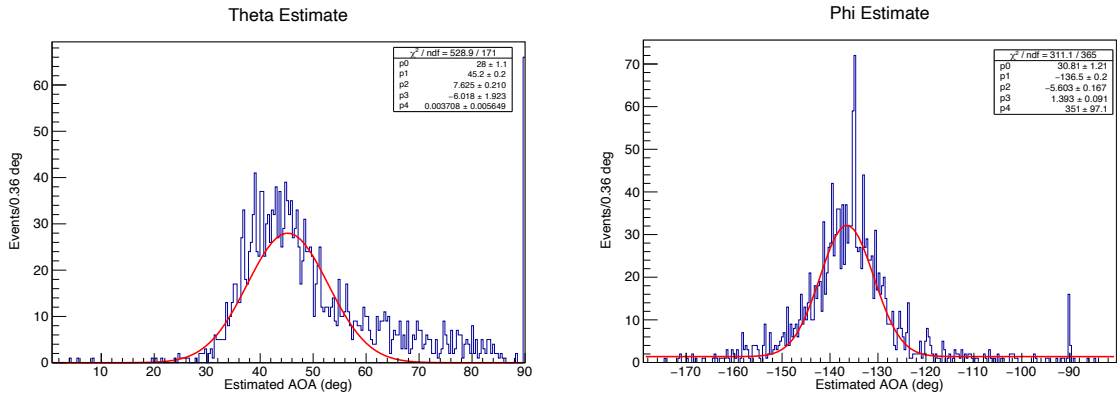

Figure 33. AOA estimation with emulated 3 mm drift gap detector

These spurious 90° results are the result of attempting to compute an AOA when too few drift gap gas molecules have been ionized to generate at least 2 detections on both the x and y readout strips. In the absence of 2 detections, there is not enough information to compute a slope. An estimate of the chance of this event is shown in Table 5 below. The calculation in this table is based on an average of 20 gas ionizations with a 16 mm drift gap (see Figure 7), assuming that the average number of ionizations scales with drift gap width, and an assumption that ionizations are Poisson distributed. This table indicates that at least 11% of the events would result in this anomalous result.

Table 5. Probability of ionizations for 3 mm drift gap

Ionizations	Probability	Cumulative
0.	0.024	0.024
1.	0.088	0.112
2.	0.165	0.277
3.	0.207	0.484
4.	0.194	0.678
5.	0.145	0.823
6.	0.091	0.914

To verify that these anomalous results were due to cases in which there were too few ionizations to generate a slope, the data were run again, but only events for which both the x and y channels experienced greater than 1 detection were counted. Figure 34 shows the result with this restriction. The absence of a spike in the histogram of θ in this figure justifies the assumption that the anomalies are due to too few ionizations.

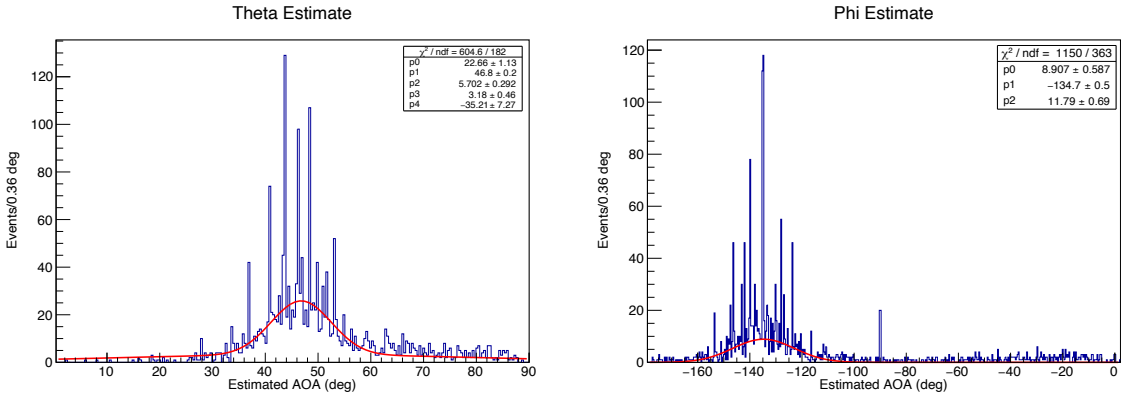

Figure 34. AOA estimation for events with more than 1 ionization

When the angle of incidence of the beam track is reduced from 45°, the effect of a 3 mm drift gap is even more pronounced. Much of this impact is the result of a higher probability of fewer than 2 ionizations in the drift gap. This is due primarily to the fact that the length of the particle track in the drift gap is shorter as the angle of incidence reduces. Table 6 shows the computed probability of fewer than 2 ionizations for smaller angles of incidence. This can be seen in the histograms of the estimate of θ in Figure 35 where when the angle of incidence changes between 30° and 15°.

Table 6. Events with too few ionizations

Beam Angle of Incidence	Fraction of Events with Fewer Than 2 Ionizations
15°	24%
30°	19%
45°	11%

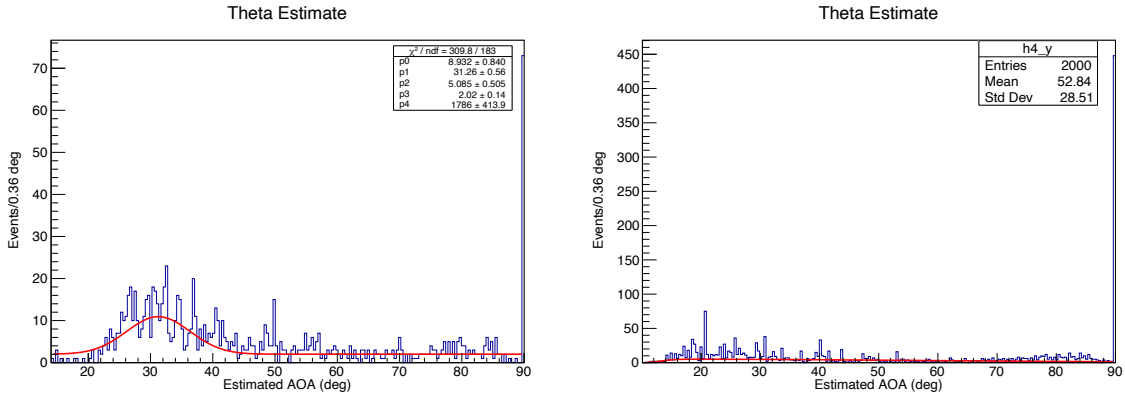

Figure 35. Impact of beam incident angle on anomalous (AOA=90°) AOA estimation (left plot for θ = 30°; right plot for θ = 15°)

Although, based on these estimates, the current lab detector does not appear to provide a useful estimate of AOA, the same emulation approach can be used to estimate the resolution performance of a range of detectors with drift gap widths between 3 mm and 16 mm. The result of this evaluation is shown in Figure 36 below. For this evaluation, the resolution was computed using histograms with only events having 2 or more ionizations. With the exception of the case of 45° angle of incidence, limiting the events to only those with at least 2 ionizations did not produce a reliable estimate of the AOA. The AOA results for the other angles of incidence are shown for gap widths of 6 mm and above. As seen in Table 7 the impact of fewer than 2 ionizations on the results is negligible with drift gap widths greater than 6 mm.

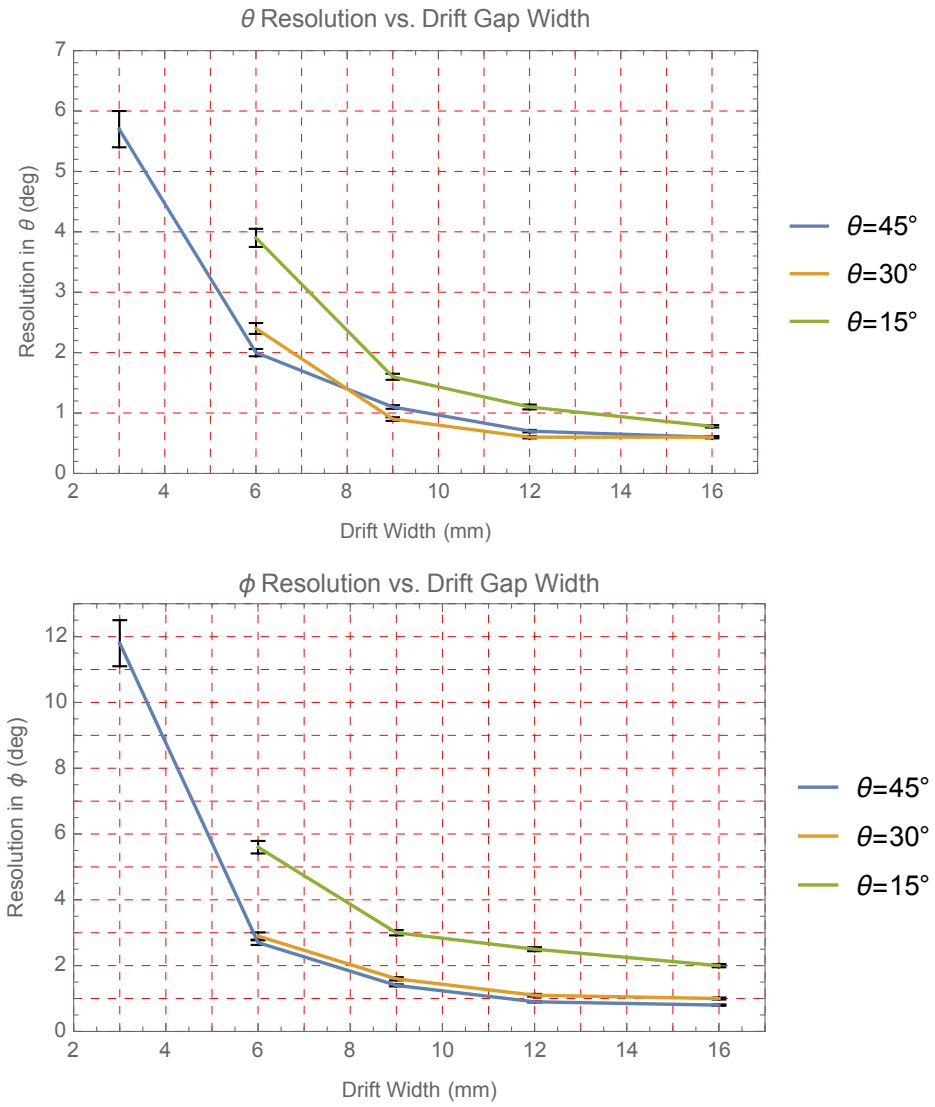

Figure 36. Impact of drift gap width on expected AOA resolution

As can be seen from the figure, just increasing the drift gap from 3 to 6 mm has a large effect on improving the resolution. Increasing the gap width above 12 mm has little additional impact on the resolution. The resolution curve is roughly equivalent to a resolution that is inversely proportional to the drift width. The inverse proportionality would be exact if only 2 ionizations contributed to the slope. The difference from inverse proportionality is likely due to additional noisy detections contributing to the slope determination and to an actual angular spread in the beam track contributing to a non-zero floor in the measured resolution.

Table 7. Probability of too few ionizations for AOA estimation

Beam Angle of Incidence	3 mm Drift Gap	6 mm Drift Gap	9 mm Drift Gap
15°	24%	3%	0.2%
30°	19%	2%	0.1%
45°	11%	0.5%	0.0%

Conclusions

This paper documents the results of a study to estimate the direction of arrival of an incoming charged particle. Based on the results of these calculations it appears that when using a GEM detector with a drift region whose depth is 16 mm, the direction of arrival of an incoming charged particle can be computed in most cases with a resolution of on the order of between 0.5° and 1°. In addition to a random error, however, there appears to be an offset in the mean in the estimation of direction of arrival from the assumed true value. The reason for this offset is unknown. It is possible that the actual true value is offset from its assumed value due to experimental misalignment. It may also be that the algorithm used to measure the time of arrival of detected pulses introduces a bias in the estimated angle. If a bias is introduced in the pulse time of arrival algorithm, it may be possible that these biases can be calibrated out.

The estimation of direction of arrival based on measuring time of arrival of detected pulses does not yield satisfactory result when the incoming particle beam is aligned with either of the readout strips. An alternate approach for estimating the direction of arrival is necessary in these cases. Some simple alternates were investigated, but their performance was inferior to approaches using measured pulse time of arrival, both in random variations and in mean offset.

Using the data measured by BNL, an estimate of the impact that the drift gap width has on the computed AOA resolution was computed. Based on these computations, it was found that at least a 6 mm drift gap is required to even be capable of reliably estimating AOA and that, while a 16 mm drift gap enables the AOA estimate with the best resolution, most of the improvement in resolution as a function of drift gap width is achieved with a 9 mm drift gap.

Acknowledgement

We want to thank M. Purschke and B. Azmoun from the BNL group for making their data and analysis code available to us for this analysis.

References

[1] F. Sauli, "The gas electron multiplier (GEM): Operating principlesand applications," *Nuclear Instruments and Methods inPhysics Research A,* pp. 2-24, 2016.

[2] B. Azmoun, et. al., "A Study of a Mini-Drift GEM Tracking Detector," *IEEE Transactions on Nuclear Science,* vol. 63, no. 3, pp. 1768-1776, 2016.

[3] Fermilab, "Beam Structure and Delivery Path," [Online]. Available: https://ftbf.fnal.gov/beam-delivery-path/. [Accessed 19 November 2020].

[4] M. L. Purschke, BNL, *Private communication.*

[5] M. L. Purschke, et. al., "Test beam study of a short drift GEM tracking detector," in *2013 IEEE Nuclear Science Symposium and Medical Imaging Conference (2013 NSS/MIC)*, Seoul, 2013.

[6] F. Sauli, "Principles of Operation of Multiwire Proportional and Drift Chambers" CERN Report 77-09, 3 May 1977.

[7] B. Azmoun, BNL, *Private communication*.

[8] Wikipedia, "Rice distribution," [Online]. Available: https://en.wikipedia.org/wiki/Rice_distribution/. [Accessed 13 September 2021].